

# Structural and vibrational properties of $(\text{InAs})_m(\text{GaAs})_n$ strained superlattices grown by molecular beam epitaxy

G. Scamarcio, O. Brandt, L. Tapfer, D. J. Mowbray, M. Cardona, and K. Ploog  
*Max-Planck-Institut für Festkörperforschung, D-7000 Stuttgart 80, FRG*

(Received 23 July 1990; accepted for publication 17 September 1990)

The structural and vibrational properties of superlattices composed of many periods of highly mismatched InAs and GaAs layers have been studied by means of x-ray diffraction and Raman scattering as a function of the sample geometry. X-ray diffraction measures the average lattice mismatch between the superlattice and the substrate. The long-range order influences the propagative acoustic phonons whereas strain and confinement effects compete in determining the optic vibration frequencies of the InAs layers. The linewidth of the main superlattice peak in the diffraction patterns and the scattering intensities of the acoustic phonons are related to the actual shape of the interfaces. We find that the stability of the structures depends on the total number of periods, in agreement with the predictions of equilibrium elasticity theory. However, the competition between the different relaxation processes is governed by the individual layer thicknesses.

## I. INTRODUCTION

The pseudomorphic growth of highly strained superlattices is severely limited by the lattice mismatch between the constituent materials.<sup>1</sup> Particularly, energy balance considerations show that upper limits exist for the individual layers as well as for the total thicknesses of multiple heterostructures, above which the strain can no longer be accommodated entirely by elastic distortion of the layers but is relieved by the formation of misfit dislocations.<sup>2</sup> The growth of InAs on GaAs is strongly influenced by the large lattice mismatch  $\{[a(\text{InAs}) - a(\text{GaAs})]/a(\text{GaAs}) = 7.16\%\}$ . The nucleation of this system switches from 2D-layer-by-layer growth to 3D-island formation (Stranski-Krastanov growth), this change occurring already after the deposition of one InAs monolayer.<sup>3,4</sup> The tendency to phase segregation in this system<sup>5,6</sup> favors interdiffusion processes, which represent an additional strain relief mechanism competing with plastic deformation. All these effects can strongly influence the structural and vibrational properties of InAs/GaAs superlattices. However, to our knowledge, no systematic study of these effects as a function of the sample geometrical configuration exists.

The aim of this work is to study the structural and vibrational properties of InAs/GaAs superlattices as a function of the sample parameters. We investigate, by means of x-ray diffraction and Raman scattering, a series of  $(\text{InAs})_m(\text{GaAs})_n$  superlattices with individual layer thicknesses and total number of periods ranging over a wide range of values. The InAs layer thickness is kept below the individual layer critical thickness so that no strain relaxation is expected to occur at the internal interfaces. We find that the overall stability of InAs/GaAs superlattices depends on the total number of periods as predicted by energy balance models.<sup>2</sup> Taking advantage of the complementarity of x-ray and Raman spectroscopies we obtain information about the influence of the sample geometrical parameters on the relative contribution of the different strain relaxation mechanisms.

## II. EXPERIMENT

The InAs/GaAs structures were grown on semi-insulating (001) GaAs and InP substrates in a three-vacuum-chamber MBE system, equipped with elemental solid sources and an azimuthally rotating substrate holder. The substrate rotation is synchronized to the shutter operation by using an integer number of rotations per growth time for each constituent layer. Prior to the growth of the superlattice structures, a 1- $\mu\text{m}$ -thick GaAs ( $\text{Ga}_{0.47}\text{In}_{0.53}\text{As}$ ) buffer layer is deposited on the GaAs (InP) substrates, respectively. By measuring the thicknesses of test layers by means of x-ray and transmission electron microscopy we precisely calibrated the In flux in order to have an InAs growth rate  $\Gamma = 0.2 \text{ \AA/s}$  in the ultra-thin layer range.<sup>7</sup> The InAs layers are grown at 420 °C, whereas the GaAs buffer and barrier layers are grown at 540 °C. To avoid Indium loss, a few monolayers of GaAs are deposited at 420 °C on top of the InAs layer, before raising the temperature back to 540 °C. The reference for the calibration of the substrate temperature is given by the desorption of the native oxide at 580 °C observed in the RHEED (reflection high energy electron diffraction) pattern. The established As/Ga-flux ratio of  $j_{\text{As}_4}/j_{\text{Ga}} = 1$  corresponds to an As-stabilized surface as indicated by the sharp  $(2 \times 4)$  reconstruction during growth. The InAs layers are grown near the boundary of the In-rich region, as manifested by a sharp transition to a  $(4 \times 1)$  reconstruction for a slightly increased growth temperature of 430 °C. In order to obtain smooth and homogeneous layers and to minimize the density of atomic steps at the growth surface, the InAs layers are deposited in half-monolayer increments, annealing the surface after each deposition under  $\text{As}_4$  for 120 s at the growth temperature of 420 °C. This procedure leads to a sharpening of the reconstruction streaks in the RHEED pattern, which is interpreted as a smoothing of the growth surface and results in ideal 2D-layer-by-layer growth for the first two monolayers.

Monitoring the growth of thicker InAs layers (up to 10

ML), a transition from the well defined ( $2 \times 4$ ) reconstruction to a spotty RHEED pattern at a thickness of 2.5 ML is observed, revealing the onset of three-dimensional nucleation. Consequently, the individual layer thicknesses of all the samples, except one (No. 6718), are kept below the onset of island formation.

The x-ray measurements were performed with a computer-controlled high-resolution double-crystal diffractometer and with a powder diffractometer with a post-sample curved graphite monochromator. An x-ray tube with a copper target ( $\lambda_{\text{CuK}\alpha 1} = 1.540562 \text{ \AA}$ ) was used as a source for both diffractometers. The entire x-ray spectrum between  $\theta_B = 2^\circ$  and  $\theta_B = 55^\circ$  is recorded by using the powder diffractometer. High resolution diffraction patterns are recorded in the vicinity of the symmetrical (004) and the asymmetrical (224) and (115) GaAs reflections with the double crystal diffractometer.

The Raman spectra were recorded in backscattering geometry at room temperature using the discrete lines of an  $\text{Ar}^+$  laser as an excitation source while keeping the samples in vacuum in order to prevent scattering by air. In this range of excitation frequencies the penetration depth of light in InAs and GaAs is about 200–250  $\text{\AA}$  and 800–900  $\text{\AA}$ , respectively.<sup>8</sup> Therefore, no significant signal from the GaAs substrate is expected. The scattered light was dispersed by a 0.75 m double spectrometer and detected by standard photon counting followed by computer acquisition. A spectral resolution of  $\approx 2.5 \text{ cm}^{-1}$  was used. The incident photon polarization was parallel to the (110) direction while that of the scattered light was not analyzed. Typical counting rates of some  $10^2$  counts/s and signal-to-noise ratio of about 5% was measured for the acoustical phonon bands. Counting rates of some  $10^3$  counts/s were measured for the main optical phonon bands.

### III. STRAIN CALCULATION

Let us consider a pseudomorphic superlattice with a total thickness  $D_1$  of material 1 and  $D_2$  of material 2. By definition, the misfit  $\Delta$  is entirely accommodated by elastic distortion of the unit cells in the individual layers:

$$\Delta = \frac{a_2 - a_1}{\langle a \rangle} = \epsilon_{xx,1} - \epsilon_{xx,2}, \quad (1)$$

where  $\epsilon_{xx,i}$  is the strain parallel to the superlattice planes. The balance condition between the planar forces in the alternating layers gives<sup>9</sup>

$$\epsilon_{xx,1} = \frac{G_2 D_2}{G_1 D_1 + G_2 D_2} \Delta, \quad (2)$$

$$\epsilon_{xx,2} = -\frac{G_1 D_1}{G_1 D_1 + G_2 D_2} \Delta, \quad (3)$$

where the  $G_i$ 's are the shear moduli

$$G = c_{11} + c_{12} - \frac{2(c_{12})^2}{c_{11}}, \quad (4)$$

and the  $c_{ij}$ 's are the elastic stiffness constants. The case of pseudomorphic growth of the superlattice onto the substrate corresponds to  $D_1 = \infty$ .

The strain parallel to the growth axis is

$$\epsilon_{zz} = -\frac{2c_{12}}{c_{11}} \epsilon_{xx}. \quad (5)$$

## IV. RESULTS

### A. X-ray measurements

Figure 1 shows the experimental (a) and simulated (b) x-ray diffraction patterns of sample No. 6716 recorded around the symmetrical (004) GaAs reflection. In addition to the GaAs substrate peak ( $S$ ) and the 0th order SL peak ( $SL_0$ ) the spectra exhibit satellite peaks up to the 4th order, demonstrating the high periodicity of the structure. The perfect agreement between the experimental patterns and those calculated using the dynamical diffraction theory<sup>10</sup> indicates an excellent structural quality and allows us to accurately determine the InAs and GaAs individual layer thicknesses as 2.8  $\text{\AA}$  (0.8 ML) and 113  $\text{\AA}$ , respectively. This means an incomplete InAs monolayer coverage. Recording the diffraction patterns around the asymmetric (224) and (115) reflections, we find that the in-plane lattice constant  $a_{\parallel}$  of the superlattice coincides with that of GaAs. Thus, the lattice mismatch is entirely accommodated by an elastic distortion of the InAs unit cell, which becomes elongated in the [001] direction. The in-plane strain in the InAs layers is  $\epsilon_{xx} = \epsilon_{yy} = [a(\text{GaAs}) - a(\text{InAs})]/a(\text{InAs}) = -6.68 \times 10^{-2}$  while Eq. (5) gives  $\epsilon_{zz} = 7.26 \times 10^{-2}$ .

Figure 2 shows the diffraction patterns of sample No. 6722 around the symmetric (004) (a) and the asymmetric (115) (b) reflections, respectively. These allow us to determine the average lattice mismatch between the superlattice and the substrate perpendicular ( $\delta_{\perp} = 1.03 \times 10^{-2}$ ) and parallel ( $\delta_{\parallel} = 3.86 \times 10^{-4}$ ) to the (001) plane.<sup>10</sup> The ratio  $\delta_{\parallel}/\delta_{\perp}$  has a value 0 for perfectly coherent growth and 1 for

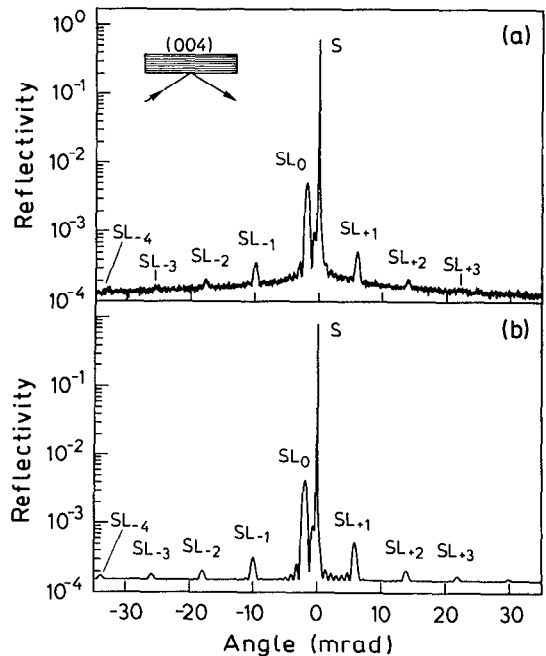


FIG. 1. Experimental (a) and simulated (b) x-ray diffraction patterns in the vicinity of the symmetrical (004) reflection for sample No. 6716.

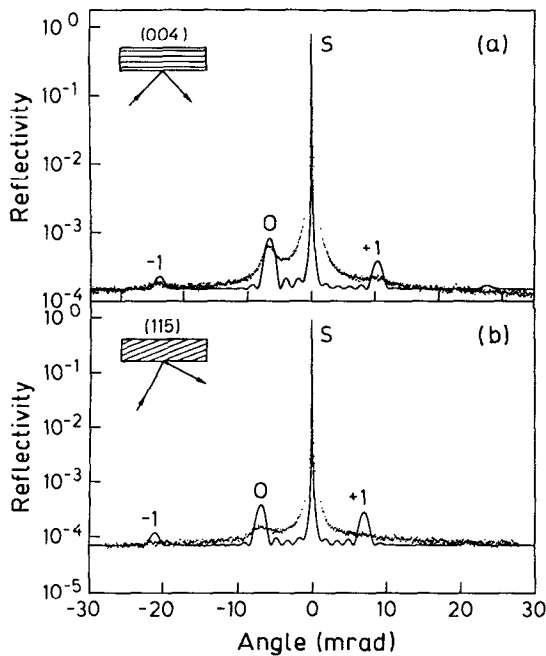


FIG. 2. Experimental (dotted line) and simulated (solid line) x-ray diffraction patterns recorded in the vicinity of the symmetric (004) (a) and the asymmetric (115) (b) reflection for sample No. 6722.

completely relaxed epilayers. Since we have kept the individual InAs layer thickness below its critical value and the  $\delta_{\parallel}/\delta_{\perp}$  ratio is very small in sample No. 6722, we can assume that the superlattice is pseudomorphic and characterized by its own lattice constant  $a_{\parallel}$ . In the frame of this approximation the strain in the GaAs layers is equal to  $\delta_{\parallel}$  while that in the InAs layers can be deduced from Eq. (1). These values are used to simulate the diffraction patterns shown in Fig. 2 in the framework of the dynamical theory. Although good agreement is found for the angular positions of the superlattice peaks between the experimental and simulated spectra, the full widths at half maxima (FWHM) and the intensities are not well reproduced. This can be attributed to incoherent x-ray scattering from crystal defects such as dislocations and clusters and indicates a certain amount of strain relaxation. By assuming that the excess strain is mainly relaxed by misfit dislocations at the superlattice/substrate interface it is possible to estimate an upper limit for their density. In fact, the in-

plane lattice mismatch  $\delta_{\parallel}$  is directly related to the misfit dislocation density  $\rho_I$ .<sup>11</sup> Assuming that the dislocations formed are all of the 60° type  $(a/2)\langle 110 \rangle$ ,<sup>12,2</sup> we have:

$$\rho_I = \epsilon_{xx} [\cos \theta \times b]^{-1}, \quad (6)$$

where  $b$  is the size of the Burgers vector and  $\theta$  is the angle between the dislocation line and the Burgers vector. We find  $\rho_I = 2.0 \times 10^{-4}/\text{cm}$  for the sample No. 6722.

For structurally perfect superlattices excellent agreement between the experimental and theoretical linewidth and intensity of the  $SL_0$  peak is observed (see Fig. 1). The line broadening of the main superlattice peak  $SL_0$  in the x-ray spectra of Fig. 2(a and b) indicates that strain relaxation also creates defects, such as dislocations or clusters, at the internal InAs/GaAs interfaces. If the peak broadening is caused by dislocations then the average dislocation density  $N$  in the superlattice is related to the linewidth broadening  $\Delta\omega$  by<sup>13</sup>

$$N = \left( \frac{\Delta\omega}{4b} \right)^2, \quad (7)$$

which gives  $N = 1.0 \times 10^8/\text{cm}^2$  for sample No. 6722. Following the same procedure we analyze the diffraction patterns of samples Nos. 6720 and 6721. The results are summarized in Table I.

It is interesting to compare samples Nos. 6721 and 6722 in which the total superlattice thicknesses as well as the amount of In are equal, but the InAs layers are separated by 20 and 10 GaAs monolayers, respectively. The in-plane lattice mismatch in sample No. 6722 is twice that of sample No. 6721, but the average dislocation density in the former superlattice is only one third that of the latter. This indicates that in the sample with thicker InAs layers the strain relaxation is favored at the first InAs/GaAs interface, resulting in a reduction of strain in the rest of the structure.

The superlattice peaks in the x-ray spectra of samples Nos. 6718 and 6719 are too weak to be detected by means of the double crystal diffractometer. This fact and the broadening of the main epilayer peak are indicative of a rather poor structural quality and suggest a large amount of  $\text{Ga}_{1-x}\text{In}_x\text{As}$  alloy formation. The angular distance between the epilayer and the substrate peaks gives average In mole contents  $x = 0.43$  and  $x = 0.77$  for samples Nos. 6719 and 6718, respectively.

Table I summarizes the structural properties deduced

TABLE I. Structural parameters of the investigated series of  $(\text{InAs})_m(\text{GaAs})_n$  superlattices. Here  $d$  = superlattice period measured by x-rays (first value) and Raman (second value), respectively;  $\delta_{\parallel}$ ,  $\delta_{\perp}$  = average lattice mismatch parallel and normal to the (001)-plane, respectively;  $\rho_I$ ,  $N$  = maximum misfit dislocation density at the superlattice/substrate interface and in the superlattice, respectively;  $x$  = mean In mole fraction and  $N_c$  = critical number of periods.

Sample No.	$N(m,n)$	substrate	$d(\text{\AA})$	$\delta_{\parallel} (\times 10^{-4})$	$\delta_{\perp} (\times 10^{-2})$	$\rho_I (\times 10^4/\text{cm})$	$N (\times 10^8/\text{cm}^2)$	$x$	$N_c$
6716	10(1,40)	(001)-GaAs	115.8	0	0.284				9.3
6722	10(2,20)	"	53.4/52.2	3.86	1.03	2.0	1.0		3.6
6721	20(1,10)	"	23/25	2.06	1.43	1.0	3.5		7.2
6720	10(2,10)	"	26/26	31.5	2.23	16	30		3.1
6719	100(2,2)	"			3.0		30	0.43	
6718	100(10,2)	"			5.11		14	0.77	
5736	800(2,2)	(001)-InP	11.0/11.3		0.826				

by x-ray measurements for the complete series of investigated samples.

## B. Raman measurements

Because of the influence of the layer thickness, strain, and chemical composition on the superlattice vibrations, Raman scattering can provide information about the structural properties of heterostructures analogous, and in some cases complementary, to that obtained by x-ray diffractometry.<sup>14</sup> The folded acoustic modes are mainly sensitive to the long-range order in the superlattice whereas the confined optical phonons are influenced by details of the individual layers. In addition, propagative optical modes may exist when the phonon dispersion curves of the two materials are superimposed in energy.

### 1. Acoustic phonons

The folded acoustic modes appear at the Brillouin zone center as closely spaced doublets whose average frequency  $\Omega$  is related to the superlattice period  $d = d_A + d_B$  by<sup>15</sup>

$$\Omega_\nu = \frac{2\nu\pi v}{d}, \quad \nu = 0, 1, 2, \dots, \quad (8)$$

where  $v = [\alpha/v_B + (1 - \alpha)/v_A]^{-1}$  is the average sound velocity in the superlattice and  $\alpha = d_B/d$ .

Figures 3(a, b, and c) show the Raman spectra in the acoustic region for samples Nos. 6722, 6720, and 6721, respectively. In the backscattering configuration one does not observe the phonons with exactly  $k = 0$  but those with  $k = \pm 4\pi n/\lambda$  where  $n$  is the refractive index of the material and  $\lambda$  the wavelength in vacuum. This produces a splitting of

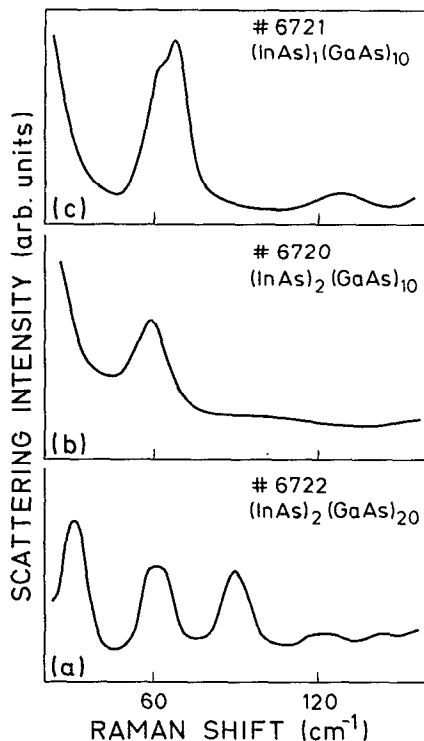


FIG. 3. Raman spectra recorded at RT under 4880 Å excitation in the acoustic phonon region for the samples indicated in the figure.

the frequencies  $\Omega_\nu$  into  $\Omega_\nu \pm 4\pi\nu v/\lambda$  where usually both components have comparable intensities.

The four equally spaced peaks positioned at 29.5, 59.5, and 88.5  $\text{cm}^{-1}$  and the broad band around 120  $\text{cm}^{-1}$  in Fig. 3(a) are due to the first four doublets, here unresolved, of the folded longitudinal acoustic (LA) modes of sample No. 6722. Due to the small value of  $\alpha$ , the elastic properties of the structure are dominated by those of GaAs. An experimental value of  $v_A = 4.726 \text{ m/s}$ <sup>16</sup> is available for the GaAs sound velocity in the  $\{100\}$  directions. The sound velocity of InAs can be calculated to be  $v_B = \sqrt{c_{11}/g} = 3.833 \text{ m/s}$  from the known values of the elastic stiffness constant  $c_{11}$  and density  $g$ ,<sup>17</sup> and neglecting the effect of strain. Accordingly, a superlattice period  $d = 52 \text{ Å}$  is deduced, in very good agreement with the x-ray value. Analogously, the band peaked at 57.5  $\text{cm}^{-1}$  in Fig. 3(b) and those centered at 64.5  $\text{cm}^{-1}$  and 130  $\text{cm}^{-1}$  in Fig. 3(c) are due to LA doublets and correspond to periods of  $d = 26 \text{ Å}$  and  $d = 24 \text{ Å}$  for samples Nos. 6720 and 6721, respectively, again in excellent agreement with the x-ray values.

In contrast with their frequencies, the intensity of the folded lines are sensitive to the compositional profile of the structure, being proportional to the square of the Fourier components of this profile.<sup>18</sup> In particular, for abrupt interfaces, the Fourier components decrease slowly with increasing order. Also, numerical calculations show that the intensities of the folded acoustical modes depend on the ratio  $d_2/(d_1 + d_2)$ .<sup>19</sup> Again, it is interesting to compare the two samples Nos. 6722 and 6721 in which the ratio  $d_2/(d_1 + d_2)$ , as well as the total superlattice thicknesses, are equal. The very small decrease in the intensity of the higher order peaks in Fig. 3(a), as compared with the corresponding trend in Fig. 3(c), is suggestive of much sharper interfaces in sample No. 6722 than in sample No. 6721. This, in turn, suggests a higher amount of interdiffusion in the latter sample. Analogously, the lack of higher order peaks in Fig. 3(b) indicates a poor interface quality in sample No. 6720.

A common feature of the bands observed in Figs. 3(a, b, and c) is that they are rather broad (much broader than the spectral resolution) and the folded acoustic doublets cannot be resolved. This fact can be attributed to fluctuations in the superlattice period. Since this also occurs in GaAs/InAs superlattices grown on InP substrates<sup>20</sup> (see also Fig. 5) it should have an intrinsic nature and can be related to the tendency to phase segregation at the InAs/GaAs interfaces.

### 2. Optic phonons

The frequencies of the main optic phonons of a superlattice are determined both by the confinement and the strain in the individual layers. According to the usual linear chain approximation<sup>21</sup> the modes confined in the phonon potential well can be described as standing waves whose frequencies are those of the bulk corresponding to wave vectors

$$k_m = \frac{\pi}{(n+1)a} m, \quad m = 1, \dots, n, \quad (9)$$

where  $a$  is the lattice constant and  $n$  is the number of monolayers in a single slab. Since the optical phonons in III-V compounds have negative dispersions, the confinement ef-

fect always results in a red-shift of the superlattice peaks with respect to the bulk frequency.

Biaxial strain induces a shift  $\Delta\omega$  of the longitudinal optic (LO) frequencies described by<sup>22</sup>

$$\frac{\Delta\omega}{\omega} = \frac{K_{11}}{2} \epsilon_{zz} + \frac{K_{12}}{2} (\epsilon_{xx} + \epsilon_{yy}) \quad (10)$$

where  $K_{ij}$  are anharmonic spring constants and  $\epsilon_{xx} = \epsilon_{yy}$ ,  $\epsilon_{zz}$  are the components of the strain tensor in the individual layers. According to the signs of the strain components either a red- or a blue-shift results.

Figures 4(a-f) show the Raman spectra in the optic phonon region of the complete series of  $(\text{InAs})_m(\text{GaAs})_n$  superlattices recorded under 4880 Å excitation which is close to resonance with the  $E_1$  gap of bulk InAs.<sup>23</sup>

The strong bands labelled  $\text{LO}_G$ , dominating the spectra of Fig. 4(a-d), originate from the GaAs-like longitudinal optic modes confined in the GaAs layers. The peak positions are 291.5, 289.1, 288.5, and 289.2  $\text{cm}^{-1}$  in Fig. 4(a, b, c, and d), respectively. The small red-shift of the  $\text{LO}_G$  frequencies with respect to that of bulk GaAs LO (291.6  $\text{cm}^{-1}$ ) is consistent with the small expected confinement effect for the relatively thick GaAs layers and narrow barriers and with the weak strain-induced red-shift. The values  $\Delta\omega = -0.2$ ,  $-0.1$ , and  $-1.6 \text{ cm}^{-1}$  are obtained with Eq. (11) for the LO phonons of GaAs of samples Nos. 6722, 6721, and 6720, respectively.

The weaker bands labelled  $\text{TO}_G$ , clearly observable in the magnified part of Figs. 4(a-d), are due to scattering by GaAs-like transverse optic modes. This process, forbidden in backscattering from a {100} surface can be weakly induced by disorder. The  $\text{LO}_G$  and  $\text{TO}_G$  bands become noticeably broader when passing from Fig. 4(a) to Fig. 4(d). Particularly, a tail appears to the low energy side of the  $\text{LO}_G$  band, probably due to the envelope of the higher order LO modes confined in the GaAs layers. The broadening of the  $\text{TO}_G$  peak in Figs. 4(b) and 4(c) may have a similar origin.

Additional weaker features can be observed in the spectra of Figs. 4(a-d). The broad structure around 220  $\text{cm}^{-1}$  in Fig. 4(a) is due to defect-activated (DALA) modes.<sup>24</sup> A similar feature is also observed in the Raman spectrum of an MBE grown GaAs layer recorded under identical experimental conditions.<sup>25</sup>

No detectable structure can be ascribed in Fig. 4(a) to the scattering by InAs phonons. A reduction of about two orders of magnitude in the InAs to GaAs scattering efficiency ratio is expected from considerations of the ratio between the InAs and GaAs layer thicknesses and the comparable scattering efficiencies of MBE-grown GaAs and InAs bulk samples measured at 4880 Å.<sup>25</sup>

The two broad and weak bands, positioned around 245 and 242  $\text{cm}^{-1}$  in Figs. 4(b) and 4(c), respectively, on the low energy tail of the GaAs optical phonon bands, can be ascribed to scattering by LO phonons of InAs. Their energy position, slightly higher than the bulk InAs LO frequency (238.6  $\text{cm}^{-1}$ ), is consistent with the expected competing strain and confinement effects. In fact, a strain-induced blue-shift of about 22  $\text{cm}^{-1}$  and a confinement red-shift of about 12 and 17  $\text{cm}^{-1}$  are expected for samples Nos. 6722 and

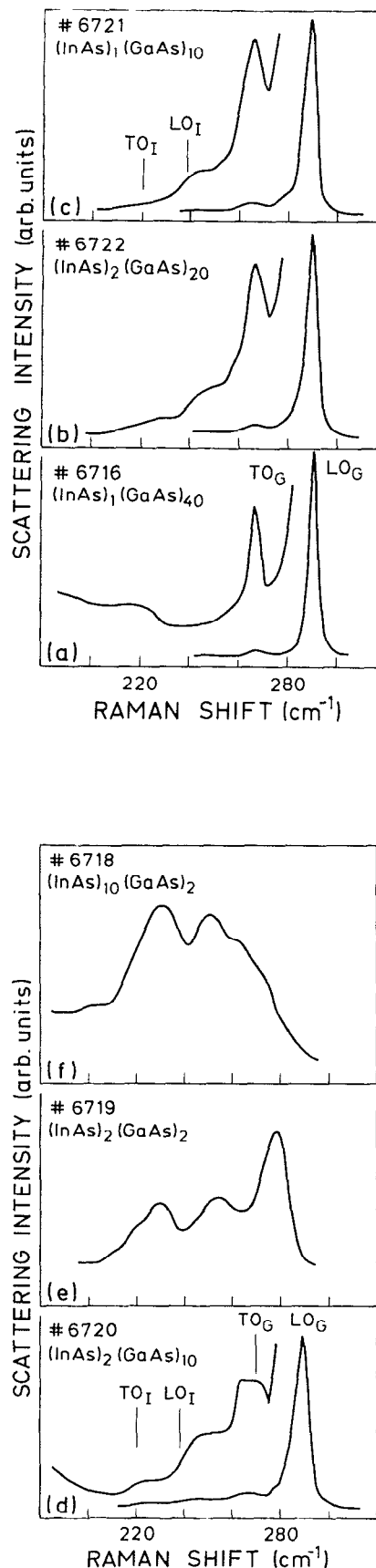


FIG. 4. Raman spectra recorded at RT under 4880 Å excitation in the optic phonon region for the samples indicated on the figure. The arrows labelled  $\text{TO}_I$ ,  $\text{LO}_I$ ,  $\text{TO}_G$ , and  $\text{LO}_G$  mark the transverse optic and the longitudinal optic phonons of InAs and GaAs, respectively.

6721, respectively. The observed band broadening can be attributed to disorder, including thickness fluctuations of the InAs monolayers, and/or to inhomogeneous strain distribution.

Several broad and weak features can be observed in Fig. 4(d), falling in the range between the bottom of the InAs and the top of the GaAs optic phonon dispersion, with a cutoff at about  $210 \text{ cm}^{-1}$ . In particular, three bands centered around  $225$ ,  $245$ , and  $278 \text{ cm}^{-1}$  and an unresolved structure superimposed on the  $\text{TO}_G$  band, can be observed. Although scattering by the strain-shifted InAs LO phonon can give a contribution to the  $245 \text{ cm}^{-1}$  band, the number and energy positions of the remaining bands are strongly suggestive of GaInAs alloy modes.

In Fig. 4(e), a shoulder around  $220 \text{ cm}^{-1}$  and three broad bands peaked at  $231.2$ ,  $255.1$ , and  $278.6 \text{ cm}^{-1}$  are observed. Their energy positions are close to the InAs- and GaAs-like TO and LO frequencies of a  $\text{Ga}_{1-x}\text{In}_x\text{As}$  alloy with  $x = 0.4$ .<sup>26</sup> Analogously, the two bands peaked at  $229$  and  $250.4 \text{ cm}^{-1}$  and the shoulder on the high energy side observable in Fig. 4(f) suggest an In-rich  $\text{Ga}_{1-x}\text{In}_x\text{As}$  alloy formation in the sample No. 6718 consistent with the x-ray value of  $x = 0.77$ .

Figure 5 shows the Raman spectrum of sample No. 5736 which is representative of a series of  $(\text{GaAs})_2(\text{InAs})_2$  superlattices grown on InP substrates. In this case the average strain is equally shared by the InAs and GaAs layers. A band peaked at  $124 \text{ cm}^{-1}$  and a strong peak at  $271.5 \text{ cm}^{-1}$  followed on the low energy side by a plateau with an edge around  $220 \text{ cm}^{-1}$ , can be observed. The frequency position of the lowest energy band is consistent with the period  $d = 11.0 \text{ \AA}$  determined with x-rays and allows us to ascribe this band to the first LA doublet. The peak at  $271.5 \text{ cm}^{-1}$  can be assigned to a GaAs-like phonon. Its energy position is mainly determined by the confinement in the 2-ML-thick GaAs layer and to a smaller extent by the strain-induced shift. The low energy tail is due to In-related phonons. Its weakness and width can be related to both disorder and GaInAs alloy formation due to the tendency to segregation of InAs.

## V. DISCUSSION

The structural stability of a strained superlattice is related to the existence of critical thicknesses for the individual strained layers ( $h_c$ ) as well as for the whole heterostructure ( $H_c$ ) above which the excess strain is relaxed. According to the model of Ref. 27 a critical thickness  $h_c = 3 \text{ ML}$  for an InAs layer grown on a GaAs substrate, can be calculated. By studying the RHEED patterns we observe a switch from the laminar to the island growth regime around 2.5 ML of InAs, under our growth conditions. Therefore, when we keep the InAs layer thicknesses below 2 ML, the structural stability of all the investigated samples, excepting No. 6718, should be governed by the total superlattice thickness and/or by interdiffusion processes.

The critical thickness  $H_c$ , or, equivalently, the critical number of periods  $N_c$ , for a strained superlattice is given in the framework of the energy balance model<sup>2</sup> by

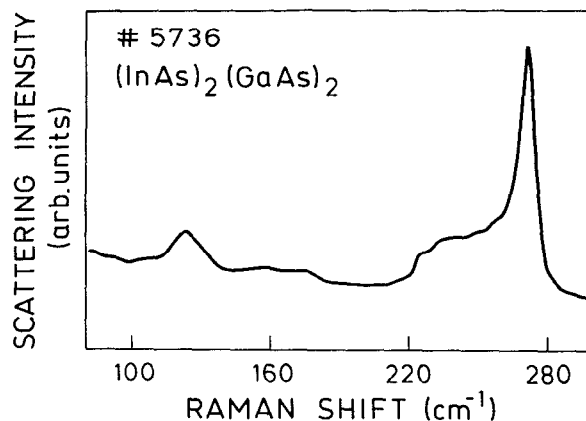


FIG. 5. Raman spectrum of sample No. 5736, recorded at RT under  $4880 \text{ \AA}$  excitation.

$$H_c = N_c d_2 = \frac{b(1 - \nu \cos^2 \theta)}{8\pi(1 + \nu)\epsilon \cos \lambda} \left[ \ln 4N_c \left( \frac{d_1 + d_2}{b} \right) \right], \quad (11)$$

where  $\nu$  is the Poisson ratio,  $\lambda$  is the angle between the Burgers vector  $b$  and the direction normal to the dislocation line, and  $\epsilon$  is the maximum in-plane strain.

The number of periods in sample No. 6716 is almost equal to the critical value  $N_c$ . Hence the excellent structural quality observed in the limit of the sensitivity of our experimental techniques, is well accounted for by the energy balance model.

When  $N_c$  is exceeded, the excess strain is relaxed by two main mechanisms, namely, misfit dislocation formation and interdiffusion. Indeed, our x-ray and Raman data can be interpreted in terms of strain relaxation processes. A structural deterioration is clearly evident for samples Nos. 6718 and 6719 in which the number of periods is by far in excess of  $N_c$ . Particularly, in the former sample the InAs critical thickness is also exceeded and an extensive structural deterioration through interdiffusion can be observed.

Although the equilibrium elasticity theory actually predicts the onset, it overestimates the amount of strain relaxation in the epilayer.<sup>27</sup> Indeed, an almost complete strain relief (about 95%) for samples No. 6720, 6721, and 6722 is predicted, in contrast with the very small strain relaxation measured by x-ray diffraction. A similar behavior, observed also in InGaAs/GaAs single heterostructures, has been mainly attributed to the difficulty in creating new dislocations (energy barriers).<sup>28</sup>

It is particularly interesting to compare samples Nos. 6722 and 6721 in which the critical thickness is exceeded by the same amount. These samples also have an equal superlattice thickness and the same ratio between the InAs and the GaAs layer thicknesses. Hence, we expect similar structural properties. Nevertheless, our results clearly show that in the sample with thicker InAs layers (No. 6722) the excess strain is mainly released by misfit dislocation formation at the substrate/epilayer interface and that sharper internal interfaces are obtained. On the contrary, in sample No. 6721 misfit dislocation formation at the internal interfaces, as well as

interdiffusion processes, are more efficient. In addition comparison between samples Nos. 6722 and 6720 show that thicker GaAs layers are more effective in stabilizing the superlattice structure. These findings are qualitatively confirmed by transmission electron microscopy measurements.<sup>29</sup> The previous discussion indicates that provided the thickness of the strained layers is below the onset for strain relaxation, the structural stability of the superlattice depends only on the total number of periods but the competition between the different relaxation mechanisms is still regulated by the individual layer thicknesses.

Finally we discuss the sample No. 5736 which consists of an  $(\text{InAs})_2(\text{GaAs})_2$  structure grown on InP substrates. In this case the strain between the constituent layers and the substrate is equally shared by the InAs and GaAs layers, resulting in a very small net-strain superlattice whose total thickness should not be limited by structural instability. Both x-ray and Raman data reveal the periodicity of the structure. However, the Raman spectra show substantial alloy formation. This can be explained by the large excess energy of the stretched Ga—As bonds and the compressed In—As bonds which causes interdiffusion processes at the internal superlattice interfaces, representing a local strain relief mechanism independent of the net-strain in the structure.

## VI. CONCLUSIONS

Our results clearly document the complementarity of x-ray diffraction and Raman scattering in studying the structural and vibrational properties of highly mismatched InAs/GaAs superlattices. While x-ray diffraction measures the average lattice mismatch between the superlattice and the substrate, scattering by optical phonons shows a competition between strain and confinement effects in the individual layers and is particularly sensitive to alloy formation. The periods of the structures are given by the peak positions in both x-ray and Raman spectra. Information about the dislocation formation and the interface sharpness can be obtained by studying the linewidth broadening of the main superlattice peak in the diffraction patterns and the scattering intensities of the folded acoustic phonons, respectively. One important finding is that the structural stability of InAs/GaAs superlattices is related to the total number of periods, in agreement with the predictions of elasticity theory, whereas the competition between the strain relaxation mechanisms, namely dislocation formation and interdiffusion, is governed by the individual layer thicknesses.

## ACKNOWLEDGMENTS

This work has been partly supported by the Bundesministerium für Forschung und Technologie of the Federal Republic of Germany. One of us (DJM) acknowledges financial support from the Alexander von Humboldt Foundation (Bonn, Federal Republic of Germany).

- <sup>1</sup> For a recent review see C. Mailhot and D. L. Smith, *Crit. Rev. Solid State Mater. Sci.* **16**, 131 (1990).
- <sup>2</sup> D. C. Houghton, D. D. Perovic, J. -M. Baribeau, and G. C. Weatherly, *J. Appl. Phys.* **67**, 1850 (1990).
- <sup>3</sup> F. Houzay, C. Guille, J. M. Moison, P. Henoc, and F. Barthe, *J. Crystal Growth* **81**, 67 (1987).
- <sup>4</sup> W. J. Schafer, M. D. Lind, S. P. Kovalczyck, and R. W. Grant, *J. Vac. Sci. Technol. B* **1**, 688 (1983).
- <sup>5</sup> C. Guille, F. Houzay, J. M. Moison, and F. Barthe, *Surf. Sci.* **189/190**, 1041 (1987).
- <sup>6</sup> J. T. Ebner and J. R. Arthur, *J. Vac. Sci. Technol. A* **5**, 2007 (1985).
- <sup>7</sup> O. Brandt, L. Tapfer, R. Cingolani, K. Ploog, M. Hohenstein, and F. Philipp, *Phys. Rev. B* **41**, 12599 (1990).
- <sup>8</sup> E. D. Palik and R. T. Holm, in *Handbook of Optical Constants of Solids*, edited by E. D. Palik (Academic, New York, 1985).
- <sup>9</sup> B. Jusserand and M. Cardona, *Light scattering in solids V*, edited by M. Cardona and G. Guntherodt (Springer, New York, 1988), p. 145.
- <sup>10</sup> L. Tapfer, *Phys. Scri. T* **25**, 45 (1989).
- <sup>11</sup> S. N. G. Chu, A. T. Macrander, K. E. Strege, and W. D. Johnston, Jr., *J. Appl. Phys.* **57**, 249 (1985).
- <sup>12</sup> I. J. Fritz, *Appl. Phys. Lett.* **51**, 1080 (1987).
- <sup>13</sup> L. Tapfer, J. R. Martinez, and K. Ploog, *Semic. Sci. Tech.* **4**, 617 (1989).
- <sup>14</sup> B. Jusserand and M. Cardona, in Ref. 9, p. 119.
- <sup>15</sup> B. Jusserand, F. Alexandre, J. Dubard, and D. Paquet, *Phys. Rev. B* **33**, 2897 (1986).
- <sup>16</sup> H. J. McSkimin, A. Jayaraman, and P. Andrecht, *J. Appl. Phys.* **38**, 2362 (1967).
- <sup>17</sup> D. Gerlich, *J. Appl. Phys.* **34**, 2915 (1963).
- <sup>18</sup> D. Levi, S. L. Zhang, M. V. Klein, J. Klem, and H. Morkoç, *Phys. Rev. B* **36**, 8032 (1987).
- <sup>19</sup> B. Jusserand, D. Paquet, F. Mollot, F. Alexandre, and G. leRoux, *Phys. Rev. B* **35**, 2808 (1987).
- <sup>20</sup> J. M. Gerard, J. Y. Marzin, B. Jusserand, F. Glas, and J. Primot, *Appl. Phys. Lett.* **54**, 30 (1989).
- <sup>21</sup> B. Jusserand, D. Paquet, and A. Regreny, *Phys. Rev. B* **30**, 6245 (1984).
- <sup>22</sup> F. Cerdeira, A. Pinczuck, J. C. Bean, B. Battlog, and B. A. Wilson, *Appl. Phys. Lett.* **45**, 1138 (1984); P. Wickboldt, E. Anastassakis, R. Sauer, and M. Cardona, *Phys. Rev. B* **35**, 1362 (1987).
- <sup>23</sup> M. Cardona, K. L. Shaklee, and F. M. Pollak, *Phys. Rev.* **54**, 696 (1967).
- <sup>24</sup> H. Kawamura, R. Tsu, and L. Esaki, *Phys. Rev. Lett.* **29**, 1397 (1972).
- <sup>25</sup> G. Scamarcio, D. J. Mowbray, and O. Brandt (unpublished results).
- <sup>26</sup> M. H. Brodsky and G. Lukovsky, *Phys. Rev. Lett.* **21**, 990 (1968).
- <sup>27</sup> J. W. Matthews and A. E. Blakeslee, *J. Cryst. Growth* **27**, 118 (1974).
- <sup>28</sup> A. V. Drigo, A. Aydinli, A. Carnera, F. Genova, C. Rigo, C. Ferrari, P. Franzosi, and G. Salviati, *J. Appl. Phys.* **66**, 1975 (1989) and references therein.
- <sup>29</sup> M. Hoenstein (private communication).